Yang and Lee *Int J Concr Struct Mater* (2019) 13:50
https://doi.org/10.1186/s40069-019-0364-x

International Journal of Concrete Structures and Materials

RESEARCH Open Access

Shear Friction Characteristics and Modification Factor of Concrete Prepared Using Expanded Bottom Ash and Dredged Soil Granules

Keun-Hyeok Yang* and Kyung-Ho Lee

Abstract

The objective of this study is to assess the shear friction characteristics of lightweight aggregate concrete (LWAC) prepared using artificially expanded bottom ash and dredged soil granules. A total of 37 concrete mixtures were prepared under the classification of three series. In the first and second series, the natural sand content for replacing lightweight fine aggregates and the water-to-cement ratio varied to obtain different densities and compressive strengths of concrete. The third series was designed to estimate the effect of the maximum aggregate size on the friction resistance along the shear crack plane of the monolithic interfaces. The frictional angle of the LWAC tested was formulated as a function of the ratio of the effective tensile and compressive strengths of concrete through the expansion of the integrated mathematical models proposed by Kwon et al., based on the upper-bound theorem of concrete plasticity. When predicting the shear friction strength of LWAC, the present mathematical model exhibits relatively good accuracy, yielding the mean and standard deviation of the ratios between experiments and predictions of 1.06 and 0.14, respectively, whereas the empirical equations proposed by the AASHTO provision and Mattock underestimated the results. Ultimately, an advanced modification factor for shear design of LWAC is proposed as a function of the density and compressive strength of concrete and the maximum size of aggregates.

Keywords: lightweight aggregate concrete, shear friction, monolithic interface, modification factor

1 Introduction

Shear friction action is a primary load transfer mechanism at concrete-to-concrete interfaces found in the connections between columns and corbels, between squat shear walls and foundations, of dapped-end beams, and shear keys (ACI-ASCE Committee 426 1973). The shear friction mechanism in concrete interfaces was first identified in 1966 (Santoa and Júlio 2012), and the design codes (AASHTO 2014; ACI Committee 318 2014; *fib* 2010; EN 1992-1-1 2004) for reinforced concrete structures has progressed based on extensive test results compiled from normal-weight concrete (NWC) push-off specimens subjected to pure shear. According to the concrete plasticity and shear friction theorem, shear friction transfer capacity (τ_f) at monolithic concrete interfaces depends on the frictional angle of concrete (Committee and 426. 1973; *fib* 2010; Nielsen and Hoang 2011). This implies that the τ_f of a concrete interface without transverse reinforcement is affected significantly by the compressive strength and type of concrete (Yang et al. 2012). However, experimental studies to ascertain the shear friction characteristics of a lightweight aggregate concrete (LWAC) interface are still indistinct although the qualities of artificial lightweight aggregates have improved gradually, thereby expanding the practical ranges for the compressive strength of such concrete.

A few experimental studies (Yang et al. 2012; Tang et al. 2008; Mattock et al. 1976) demonstrated that shear cracks in LWAC interfaces primarily penetrate through aggregate particles, unlike the typical observations in

*Correspondence: yangkh@kgu.ac.kr
Kyonggi University, Suwon, Kyonggi-do, Republic of Korea
Journal information: ISSN 1976-0485 / eISSN 2234-1315

NWC interfaces that are governed by the crack propagation through a cement matrix around aggregate particles. Thus, shear friction transfer via aggregate interlock is reduced significantly along LWAC interface cracks. Most design codes (ACI Committee 318 2014; *fib* 2010; EN 1992-1-1 2004) introduce the modification factor to account for the reduced shear transfer capacity of LWAC owing to the softened aggregate interlock along the cracks in the concrete interfaces or reinforced concrete beams. ACI 318-14 (2014) adopted the modification factor proposed by Ivey and Buth (1967) which was empirically fitted using the limited test data of 26 LWAC beam specimens. However, the logicality and reliability of this modification factor remain controversial because of insufficient mathematical consensus on the shear friction transfer mechanism along crack interfaces in LWAC elements. Yang and Ashour (2011, 2015) reported that the modification specified in ACI 318-14 (2014) for the shear transfer capacity of LWAC beams must be revised to improve the safety of the shear design provision based on the rational mathematical approach to explicate the reduced friction properties along the LWAC interfaces.

Recently, various industrial by-products and waste materials such as fly ash, bottom ash, dredged soil, reservoir sludge, and oil palm shell have been used as a source material to produce artificial lightweight aggregates. The disparity in physical properties and chemical compositions of the source materials results in different particle characteristics including shape, angularity, substrate state, porosity, modulus of elasticity and strength of aggregates (ACI Committee 213 2014). The porous structure and relatively smooth substrate characteristic of lightweight aggregate particles yield poor resistance against crack propagations, and a weak interfacial transition zone with a cement matrix. Lee et al. (2019) demonstrated that lightweight aggregate concrete made using expanded bottom ash and dredged soil granules (referred to as LWAC-BS hereinafter) exhibited a faster decrease at the post-peak branch of the stress–strain curve and a higher direct tensile strength than lightweight aggregate concrete made using expanded clay and/or fly ash granules (LWAC-CF) at the same compressive strength ($f_c^{'}$) of concrete. This implies that the shear friction resistance of LWAC is affected by the type and characteristics of lightweight aggregates because the crack propagation at the pure shear plane is affected by the tensile resistance of aggregate and concrete under principal tensile stresses (Nielsen and Hoang 2011). Therefore, the type and characteristics of lightweight aggregates need to be considered carefully in investigating the shear friction properties at the LWAC interfaces and the modification factor.

As a sustainable activity in the concrete industry in response to the global requirements to conserve natural resources and curtailing the issue of natural aggregate depletion, the Korean government has strived to produce artificially expanded lightweight aggregates through the calcination process of bottom ash and dredged soil powders. This study primarily aims to evaluate the τ_f of LWAC-BS interfaces, and to assess the effect of the type of artificially expanded lightweight aggregates on the frictional angle (ϕ) of concrete. A total of 37 LWAC-BS mixtures were prepared with the test parameters of the design compressive strength (f_{cd}) and dry density (ρ_c) of concrete, water-to-cement ratio (W/C), and maximum aggregate size (d_a). The variation in ρ_c was controlled by the natural sand content (R_s) for the replacement of lightweight fine aggregates. The previous mathematical model (Kwon et al. 2017) derived based on the upper-bound theorem of concrete plasticity was applied to determine the frictional angle and modification factor of LWAC-BS. The reliability of the existing empirical equations (AASHTO 2014; Mattock 2001) and the proposed model for LWAC were examined through comparisons with the present test.

2 Research Significance

This study provides extensive data on the τ_f of monolithic LWAC interface made using expanded bottom ash and dredged soil granules. The different values for the frictional angle of concrete were examined with respect to the type of artificially expanded lightweight aggregates. The present study also confirms that the empirical equations proposed by the AASHTO provision (2014) and Mattock (2001) need to be revised because they provide a constant shear friction strength for the LWAC interface without transverse clamping forces, irrespective of $f_c^{'}$ and ρ_c. Moreover, the derived modification factor for the shear design of LWAC elements represents well the reduced shear friction resistance along the crack surface of LWAC.

3 Experimental Details

3.1 Concrete Specimens

A total of 37 LWAC-BS mixtures classified into three series were tested, as presented in Table 1. The first series included three groups categorized according to the f_{cd} at an age of 28 days as follows: L-group (18 MPa), M-group (24 MPa), and H-group (35 MPa). In each group, R_s was selected as the primary parameter, which varied from 0 to 100% at an interval of 25%, for the different values of ρ_c and tensile resistance of concrete. In the second series, W/C varied from 0.30 to 0.50 at an interval of 0.05 under fixed R_S values of 0% (S0 group) and 50% (S50 group). Thus, f_{cd} was not targeted previously in the concrete

Table 1 Range of test parameters investigated in each group of three series.

Series	Group	f_{cd} (MPa)	R_s (%)	W/C	W (kg/m^3)	C (kg/m^3)
I	L	18	0–100 @25	0.52–0.58	185	319–356
	M	24	0–100 @25	0.47–0.53	175–185	330–394
	H	35	0–100 @25	0.35–0.41	170	415–486
II	S0	Not designed	0	0.30–0.50 @0.05	120–200	400
	S50	Not designed	50	0.30–0.50 @0.05	120–200	400
III	S0-M	24	0	0.50	188	375
	S0-H	35	0	0.25	133	450
	S100-M	24	100	0.55	193	350
	S100-H	35	100	0.32	144	450

In the first series of mixtures, a marginally lower value of *W/C* was selected with the decrease in R_s (the increase in lightweight fine aggregate content) to achieve f_{cd}.

mixes of the second series. The third series was designed to examine the effect of d_a on the shear friction performance of LWAC-BS with different compressive strengths and densities. Considering the practical production of expanded bottom ash and dredged soil granules and the ASTM requirements (2013) for lightweight aggregate particles, d_a was selected as 4.75 mm, 9.5 mm, and 19 mm in each group categorized as the following four groups: S0-M ($R_S = 0\%$ and $f_{cd} = 24$ MPa); S0-H ($R_S = 0\%$ and $f_{cd} = 35$ MPa); S100-M ($R_S = 100\%$ and $f_{cd} = 24$ MPa); and S100-H ($R_S = 100\%$ and $f_{cd} = 35$ MPa). The present tests identified the concrete mixes with $R_S = 0\%$ as all-LWAC-BS and the other mixes with $R_S \geq 25\%$ as sand-LWAC-BS.

The mixture proportions of all the concrete specimens for the targeted requirements were determined in accordance with the procedure proposed by Yang et al. (2014a). The use of natural sand in LWAC strengthens the restraining action of the aggregate particles against the lateral expansion of cement pastes under axial loads, which contributes to enhancing the strength of the mortar matrix. Thus, the value of W/C in each group of the first series decreased slightly with the decrease in R_S to achieve f_{cd}, as presented in Table 1. A lower value of the unit water content (W) was designed with the increase in f_{cd} to restrict the segregation and immoderate bleeding in fresh concrete. No water-reducing agent was added in any of the concrete mixes.

In the first series, unit water content (W) was fixed as 185 kg/m^3 and 170 kg/m^3 for the L-group and H-group mixes, respectively, whereas the M-group mixes used the W of 175 kg/m^3 or 185 kg/m^3 for achieving the required slump value. In the second series mixes, W varied from 120 to 200 kg/m^3 at the constant unit cement content (C) of 400 kg/m^3 with respect to the investigated variations in W/C. The fine aggregate-to-total aggregate ratio (S/a) was fixed to be 40% for all the concrete mixes in the first and second series. In the third series, the fixed C and W/C were used for each group as follows: 375 kg/m^3 and 0.5 for S0-M; 450 kg/m^3 and 0.25 for S0-H; 350 kg/m^3 and 0.55 for S100-M; and 450 kg/m^3 and 0.32 for S100-H, respectively. A lower W/C was selected for all-LWAC mixes when compared with the companion concrete mixes with R_s of 100% at the same f_{cd}. The values of S/a in the concrete mixes of the third series varied slightly between 0.45 and 0.48 to achieve an appropriate slump without bleeding. Note that the specimens with d_a of 4.75 mm can be regarded as mortar mixtures without coarse aggregates, resulting in an S/a of 1.00.

3.2 Materials

Ordinary Portland cement (OPC) conforming to ASTM Type I [18] was used as the primary cementitious material for all mixes. Locally available artificially expanded granules were used for lightweight aggregates. The quality of the artificially expanded granules satisfies the requirements for structural lightweight aggregates specified in ASTM C330 (2013). The screened bottom ash and dredged soil powders used as source materials underwent various manufacturing processes including calcination and expansion in large rotary kilns at approximately 1200 °C. This process is almost identical to that for artificially expanded clay granules. For coarse lightweight aggregates, expanded granules with d_a of 19 mm were used for the first and second series mixes and those with d_a of 19 mm or 9.5 mm were used for the third series mixes. For all the mixes, artificially expanded granules with d_a of 4.75 mm were used for lightweight fine aggregates. In the mixes of the first and second series, natural sand with d_a of 1.2 mm was used for partially replacing the lightweight fine aggregates. In the third series mixes, natural sand with d_a of 4.75 mm was used for fully replacing the lightweight fine aggregates to examine the effect of aggregate size on the shear friction of concrete.

The physical properties of the aggregates used are summarized in Table 2. Lightweight aggregates feature a spherical shape and a porous core structure. Thus, lightweight aggregates generally possess higher water absorption and lower density than natural sand. The apparent density and water absorption were 1.0 g/cm^3 and 17.2%, respectively, for the lightweight coarse particles, and 1.1 g/cm^3 and 12.9%, respectively, for the lightweight fine particles. The apparent density of the lightweight aggregates was approximately 35% lower, whereas higher water absorptions as much as 10.8 times and 6.8 times were measured for lightweight coarse and fine aggregates, respectively, when compared with those of natural sand. The moduli of fineness of the lightweight particles with d_a of 19 mm, 9.5 mm, and 4.75 mm were 6.4, 5.9, and 4.4, respectively. The corresponding values for sand particles of 4.75 mm and 1.2 mm were 2.7 and 2.2, respectively.

3.3 Casting, Curing, and Testing

All the aggregates were prepared in a saturated surface-dry state, and dry mixed with cement in a 0.35 m^3-capacity mixer for 1 min. Lightweight aggregates were pre-wetted for 24 h and subsequently dried in the shade for 24 h. Immediately prior to mixing, the moisture content in the aggregates was measured and subsequently accounted for the calculation of the net unit water content of each mixture proportion. Distinct segregation or floating of lightweight aggregate particles was not observed during the mixing phase. The slump and air content of fresh concrete were measured in accordance with ASTM C143 and ASTM C231 (2013), respectively. The values of $f_c^{'}$ and ρ_c of the hardened concrete were measured using cylindrical specimens of dimensions 100 mm × 200 mm in accordance with ASTM C 39 and ASTM C 642 (2013), respectively. To measure the τ_f of the prepared LWAC mixes, push-off specimens were prepared with the dimensions of 300-mm wide, 820-mm high, and 120-mm thick. The area of the frictional plane under pure shear in the push-off specimens were 200 mm × 120 mm. Three specimens were prepared for each concrete mix.

All push-off specimens were tested to failure under a concentric load acting as pure shear in the shear plane of the test zone. Steel plates and hinges were installed at the top and bottom loading points that were aligned with the shear plane. The top and bottom stubs of the test specimens were strengthened with carbon fiber sheets to prevent flexural failure at the interface between the test zone and both stubs. The tests were conducted at the age of 91 days for the first and second series specimens, and at the age of 28 days for the third series specimens. All push-off specimens exhibited no shrinkage cracks until the specified ages of the tests.

Table 2 Properties of the aggregates used.

Type	Maximum size (mm)	Specific gravity	Water absorption (%)	Fineness modulus
Fine aggregate				
Expanded granules	4.75	1.1	12.9	4.4
Sand	4.75	1.6	1.5	2.7
	1.20	1.7	1.6	2.2
Coarse aggregate				
Expanded granules	19.0	1.0	17.2	6.4
	9.5	1.1	16.1	5.8

4 Test Results and Discussions

Table 3 summarizes the test results measured in each concrete mix. The compressive strength of concrete measured at the same age of push-off tests was used for the present discussion. All the mixtures with the exception of specimens S0-30, S50-30, S0-H-19, S0-H-10, S0-H-5, and S100-H-19 exhibited high slump values exceeding 150 mm. The initial slump (S_i) of LWAC tended to decrease as R_s and W/C decreased but was marginally affected by d_a. The air content of LWAC was insignificantly affected by R_s, W/C and d_a. The air content mostly ranged between 4.0 and 6.0%, and satisfied the requirements recommended for an air-entrained LWAC that is not exposed to freezing (ACI Committee 213 2014).

In general, the increasing rates of the tensile and shear resistances of concrete are lower than those of $f_c^{'}$. Most the code equations (AASHTO 2014; ACI Committee 318 2014; *fib* 2010; EN 1992-1-1 2004) for the tensile and shear transfer capacities of concrete have been proposed as a power function of $f_c^{'}$. Lee et al. (2019) demonstrated that the empirical equation for τ_f can be fitted using the parameter of $\sqrt{f_c^{'}}$ in the regression analysis of LWAC-BS test data. Thus, the following discussions are focused on the τ_f normalized by $\sqrt{f_c^{'}}$, with respect to each test parameter.

4.1 Typical Failure Mode

A typical crack propagation and failure plane of the push-off specimens is presented in Fig. 1. An initial crack suddenly appeared along the critical shear plane at the 90–95% of the peak load, indicating that the concrete specimens reached their shear friction capacities immediately after the crack occurred. No additional cracks were developed outside the shear plane. Thus, the failure of the specimens was primarily governed by the propagation of the initial single shear crack. Ultimately, the specimens were divided into two blocks at failure. The same

Table 3 Summary of test results.

Series	Group	Specimen	R_s (%)	W/C	d_a (mm)	S_i (mm)	v_A (%)	ρ_c (kg/m^3)	f_c' (MPa)	τ_f (1) (MPa)	$\frac{\tau_f}{\sqrt{f_c'}}$	$(\tau_f)_{Pre.}$			$(\tau_f)_{Exp.}/(\tau_f)_{Pre.}$		
												(2)	(3)	(4)	(1)/(2)	(1)/(3)	(1)/(4)
I	L	L-0	0	0.52	19	230	5.8	1301	27.5	3.15	0.60	1.65	1.40	2.96	1.91	2.25	1.07
		L-25	25	0.54	19	250	4.0	1409	26.2	3.23	0.63	1.65	1.48	3.11	1.96	2.19	1.04
		L-50	50	0.55	19	245	5.0	1486	25.4	3.41	0.68	1.65	1.55	3.20	2.07	2.20	1.07
		L-75	75	0.57	19	255	4.0	1528	24.8	3.87	0.78	1.65	1.63	3.23	2.35	2.38	1.20
		L-100	100	0.58	19	250	6.2	1540	23.5	4.01	0.83	1.65	1.70	3.17	2.43	2.36	1.26
	M	M-0	0	0.47	19	235	4.5	1366	34.1	3.22	0.55	1.65	1.40	3.32	1.95	2.30	0.97
		M-25	25	0.49	19	210	4.9	1491	33.4	3.66	0.63	1.65	1.48	3.58	2.22	2.48	1.02
		M-50	50	0.50	19	230	4.3	1611	33.0	3.80	0.66	1.65	1.55	3.81	2.30	2.45	1.00
		M-75	75	0.52	19	245	4.6	1641	32.4	3.87	0.68	1.65	1.63	3.84	2.35	2.38	1.01
		M-100	100	0.53	19	240	4.6	1698	32.1	4.12	0.73	1.65	1.70	3.93	2.50	2.42	1.05
	H	H-0	0	0.35	19	165	4.8	1605	46.3	3.60	0.53	1.65	1.40	4.25	2.18	2.57	0.85
		H-25	25	0.36	19	175	4.8	1667	45.8	4.09	0.60	1.65	1.48	4.40	2.48	2.77	0.93
		H-50	50	0.38	19	210	5.1	1686	44.8	4.12	0.62	1.65	1.55	4.42	2.50	2.66	0.93
		H-75	75	0.39	19	215	4.8	1757	43.8	4.41	0.67	1.65	1.63	4.56	2.67	2.71	0.97
		H-100	100	0.41	19	225	5.0	1783	43.6	4.65	0.70	1.65	1.70	4.61	2.82	2.74	1.01
II	S0	S0-50	0	0.50	19	220	4.7	1312	24.8	2.72	0.55	1.65	1.40	2.87	1.65	1.94	0.95
		S0-45	0	0.45	19	225	4.0	1288	26.4	2.86	0.56	1.65	1.40	2.89	1.73	2.04	0.99
		S0-40	0	0.40	19	205	4.5	1309	30.3	2.91	0.53	1.65	1.40	3.07	1.76	2.08	0.95
		S0-35	0	0.35	19	165	4.6	1330	33.5	3.16	0.55	1.65	1.40	3.21	1.92	2.26	0.98
		S0-30	0	0.30	19	15	5.0	1394	34.1	3.31	0.57	1.65	1.40	3.38	2.01	2.36	0.98
	S50	S50-50	50	0.50	19	250	4.5	1571	34.5	3.66	0.62	1.65	1.55	3.79	2.22	2.36	0.97
		S50-45	50	0.45	19	250	5.0	1619	38.5	2.79	0.45	1.65	1.55	4.05	1.69	1.80	0.69
		S50-40	50	0.40	19	195	5.0	1706	42.9	4.23	0.65	1.65	1.55	4.41	2.56	2.73	0.96
		S50-35	50	0.35	19	180	4.9	1727	45.7	4.61	0.68	1.65	1.55	4.55	2.79	2.97	1.01
		S50-30	50	0.30	19	40	4.9	1736	49.8	4.64	0.66	1.65	1.55	4.69	2.81	2.99	0.99
III	S0-M	S0-M-19	0	0.50	19	240	4.1	1441	25.6	3.81	0.62	1.65	1.40	3.14	1.90	2.24	1.22
		S0-M-10	0	0.50	9.5	245	4.2	1486	24.3	3.03	0.52	1.65	1.40	2.42	1.54	1.81	1.25
		S0-M-5	0	0.50	4.75	250	4.5	1498	24.1	2.51	0.47	1.65	1.40	1.85	1.41	1.66	1.36
	S0-H	S0-H-19	0	0.25	19	120	4.1	1633	36.8	4.12	0.68	1.65	1.40	4.02	2.50	2.94	1.03
		S0-H-10	0	0.25	9.5	135	4.3	1645	35.1	3.21	0.62	1.65	1.40	3.05	2.22	2.61	1.05
		S0-H-5	0	0.25	4.75	145	4.4	1606	34.3	2.87	0.46	1.65	1.40	2.25	1.76	2.08	1.27
	S100-M	S100-M-19	100	0.55	19	245	4.0	1717	29.1	4.52	0.65	1.65	1.70	3.79	2.13	2.06	1.19
		S100-M-10	100	0.55	9.5	250	4.2	1703	26.2	3.49	0.52	1.65	1.70	2.77	1.62	1.57	1.26
		S100-M-5	100	0.55	4.75	250	4.2	1722	24.8	2.81	0.46	1.65	1.70	2.08	1.40	1.36	1.35
	S100-H	S100-H-19	100	0.32	19	140	4.1	1831	39.0	4.77	0.69	1.65	1.70	4.53	2.62	2.55	1.05
		S100-H-10	100	0.32	9.5	165	4.0	1809	36.2	3.68	0.60	1.65	1.70	3.34	2.20	2.14	1.10
		S100-H-5	100	0.32	4.75	185	4.4	1881	36.1	3.24	0.51	1.65	1.70	2.62	1.85	1.79	1.23

(1) Measured shear friction strength.

(2) Predictions by AASHTO [$\tau_n = c + \mu(\rho_{vf} f_y + \sigma_x) \le \min(0.25 f_c', T_1)$,$c = 1.65$ MPa, $\mu = 1.0$, $T_1 = 6.89$ MPa for LWAC].

(3) Predictions by Mattock [$\tau_n = K_1 + 0.8(\rho_{vf} f_y + \sigma_x) \le \min(0.2 f_c', 8.3\,\text{MPa})$,$K_1 = 1.4$ MPa for all-LWAC and 1.7 MPa for sand-LWAC]; and

(4) Predictions by the present model.

failure modes were observed in all the specimens irrespective of the test parameters. The observation of the failure surfaces clearly demonstrated that crack propagation penetrated into the bulk of the lightweight aggregate particles. The failure surfaces were relatively smooth, although a slightly more squarrose surface was observed in the concrete with high volume sand content when compared with the all-LWAC specimen. The rupture of aggregate particles owing to the propagation of the single crack can result in a reduction in the aggregate interlock resistance and coefficient of friction of concrete (Mattock et al. 1976; Choi et al. 2014).

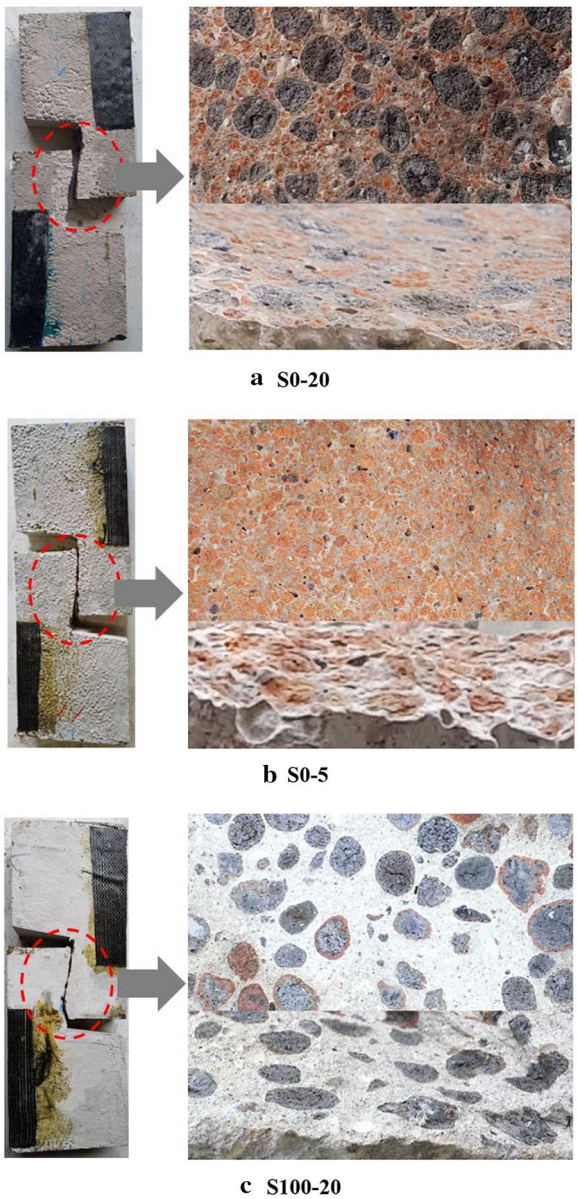

Fig. 1 Typical failure plane of push-off specimens (in series III): **a** S0-20; **b** S0-5; **c** S100-20.

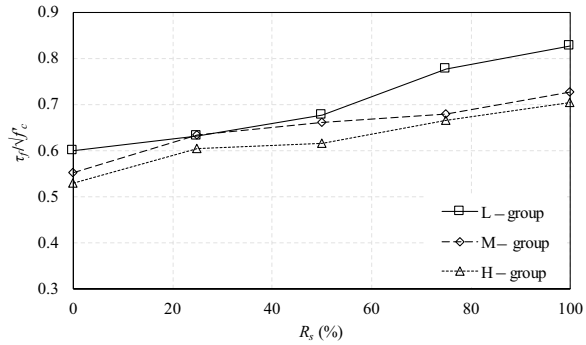

Fig. 2 Effect of R_s on τ_f/f_c' (series I specimens).

4.2 Effect of R_s (ρ_c) on τ_f/f_c'

Figure 2 shows the effect of R_s on τ_f/f_c' in the series I specimens. The value of τ_f/f_c' increased with the increase in R_s, revealing a similar increasing rate in three groups with different sand contents. When R_s increased from 0 to 100%, the increasing rates of τ_f/f_c' were 37.8%, 31.9%, and 33.1% for the L-, M-, and H-group specimens, respectively. The frictional failure of a concrete member under pure shear is critically governed by the magnitude of the primary tensile stress along the shear cracking planes. Thus, the shear and tensile capacities of concrete are indispensable to each other. This implies that the replacement of lightweight fine aggregates using natural sand is favorable for enhancing the tensile and shear friction resistances of LWAC. It is also interesting that the value of τ_f/f_c' were somewhat independent of the compressive strength of concrete, as given in Table 3.

An increase in the content of natural sand leads to the increase in ρ_c, as shown in Table 3. Thus, the increase in R_s yields an increasing ρ_c. The values of ρ_c ranged between 1301 kg/m^3 and 1540 kg/m^3, 1366 kg/m^3 and 1698 kg/m^3, and 1605 kg/m^3 and 1783 kg/m^3 for the L-, M-, and H-group specimens, respectively, indicating that a higher ρ_c is typically obtained for LWAC with a higher f_{cd}. This is because a more cement content was used in concrete mixtures with a higher f_{cd}. As aforementioned, the values of τ_f/f_c' increased with the increase in ρ_c. However, a lower τ_f/f_c' value was observed in LWAC with a higher f_{cd} at the same level of ρ_c.

4.3 Effect of W/C on τ_f/f_c'

It is commonly accepted (Yang et al. 2014a) that the decrease in W/C leads to the increase in f_c'. Thus, a higher τ_f was measured in the concrete specimens with a lower W/C, as shown in Table 3. Meanwhile, it was found that the value of τ_f/f_c' was practically independent of the W/C, as presented in Fig. 3, although extraordinarily τ_f/f_c' value was obtained in specimen S50-45. The shear friction resistance of concrete significantly depends on its compressive strength. Thus, as proposed by Lee et al. (2019), the τ_f of LWAC is approximately proportional to the square root of f_c' at the same level of ρ_c.

4.4 Effect of d_a on τ_f/f_c'

Figure 4 shows the variation in τ_f/f_c' with respect to d_a in concrete specimens with different f_{cd} and R_s values. Mortar specimens with d_a of 4.75 mm typically

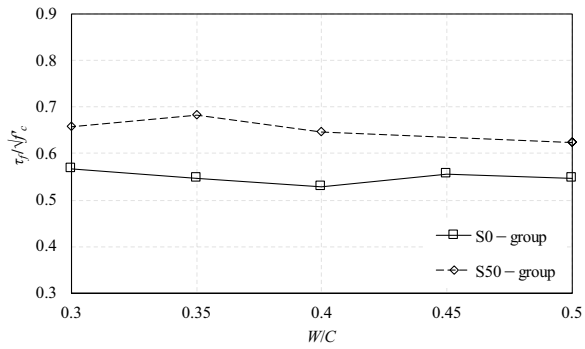

Fig. 3 Effect of W/C on τ_f/f_c'.

exhibited lower shear friction resistance than their counterpart concrete specimens. The increasing rate in τ_f/f_c' with respect to d_a was similar in both sand-LWAC and all-LWAC specimens, irrespectively of f_{cd}. When d_a varied from 4.75 mm to 19 mm, the increasing rates of τ_f/f_c' were 131% for S0-M group, 137% for S0-H group, 140% for S100-M group, and 137% for S100-H group. The shear friction resistance at the shear plane is significantly affected by the substrate roughness along the shear crack (Yang and Ashour 2011). The lightweight coarse aggregates unpierced by the crack propagation contribute to resisting the shear slip along the shear crack. Thus, a slightly higher shear friction resistance can be expected for a monolithic LWAC interface with a larger aggregate size.

5 Modeling of Shear Friction Parameters

5.1 Model Back Ground

Several researchers (Yang et al. 2012; Lee and Hong 2015; Kwon et al. 2017) proposed a mathematical model to reasonably evaluate the shear friction strength of concrete at the monolithic interfaces on the basis of the upper-bound theorem of concrete plasticity. In their model, concrete was regarded as an equivalent rigid perfectly plastic material obeying a modified Coulomb failure criteria by introducing effectiveness factors that are determined from equating the area of the rigid-perfectly plastic stress–strain curve to that of the actual stress–strain curve, as summarized in Table 4. Kwon et al. (2017) determined the effectiveness factors based on the compressive stress–strain relationship generalized by Yang et al. (2014b) and the revised version (Yang et al. 2012) of the tensile stress–strain relationship proposed by Hordijk (1991) to simulate the actual stress–strain curves of concrete. The stress–strain relationship in compression proposed by Yang et al. was fitted using the test data compiled from various types including LWAC-CF, NWC, and heavyweight concrete. Using the determined effectiveness factors, the frictional angle of concrete was formulated as a function of f_c', ρ_c, and d_a. Kwon et al. verified that the proposed model exhibits superior accuracy to the design models (AASHTO 2014; ACI Committee 318 2014; Shaikh 1978) in predicting the shear friction strength, resulting in mean and standard deviation of the ratios between the measured and predicted values of 0.95 and 0.15 for LWAC-CF, respectively. Hence, the present study expands Kwon et al. mechanical approach by adopting the compressive stress–strain relationship (Lee et al. 2019) and tensile strength fitted using the LWAC-BS data to assess the shear friction parameters of such concrete.

As summarized in Table 4, the shear friction parameters depend on the effective strengths of concrete in compression and tension. In accordance with the numerical analysis approach conducted by Kwon et al. the effectiveness factor (ν_c) for concrete in compression could be determined using the actual compressive stress–strain relationship (Lee et al. 2019) of LWAC-BS. The slopes of the ascending and descending branches of the stress–strain curves of LWAC vary with the characteristics of the lightweight aggregates and compressive strength of concrete. Thus, the stress–strain model proposed by Lee et al. needs to be examined at LWAC-BS with $f_c' > 60$ MPa.

For a parametric study to determine the shear friction parameters, LWAC-BS specimens with different ranges of $f_c' = 8$–80 MPa and $\rho_c = 800$–2300 kg/m^3, and $d_a = 4.75$–25 mm were selected in reference to the lightweight concrete classification specified in *fib* (2010). The value of ν_c was calculated for each concrete; subsequently, non-linear multiple regression (NLMR) analysis was performed to establish a simple equation. As demonstrated by Yang et al. (2012), the value of ν_c is significantly affected by f_c' and ρ_c, yet independent of d_a. The influencing variables of f_c' and ρ_c were combined and adjusted repeatedly by trial and error until a relatively high correlation coefficient

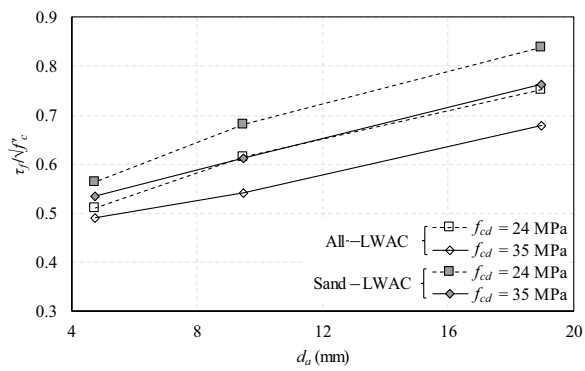

Fig. 4 Effect of d_a on τ_f/f_c'.

Table 4 Summary of shear friction strength model of LWAC.

Fundamental model: $\tau_f = \frac{1}{2} f_c^* \frac{1}{\cos\alpha}[l - m\sin\alpha]$;

$$\alpha = 2\tan^{-1}\left[\frac{x}{(x^2+y^2)^{1/2}+y}\right];$$

$$x = \frac{m}{l};\ y = \frac{(l^2-m^2)^{1/2}}{l};\ l = 1 - 2\frac{f_t^*}{f_c^*}\frac{\sin\phi}{1-\sin\phi};\ \text{and}\ m = 1 - 2\frac{f_t^*}{f_c^*}\frac{1}{1-\sin\phi}.$$

For LWAC-BS	For LWAC-CF (Kwon et al. model)
$v_c = 1.0EXP\left[-0.055\left(\frac{f_c'}{f_0}\right)\left(\frac{\rho_0}{\rho_c}\right)^{1.5}\right]$;	$v_c = 0.79EXP\left[-0.029\left(\frac{f_c'}{f_0}\right)^{0.9}\left(\frac{\rho_0}{\rho_c}\right)^{1.6}\right]$;
$\frac{f_t^*}{f_c^*} = 0.11\left[\left(\frac{f_c'}{f_0}\right)^{0.8}\left(\frac{c_0}{d_a}\cdot\frac{\rho_0}{\rho_c}\right)\right]^{-0.83}$;	$\frac{f_t^*}{f_c^*} = 0.064\left[\left(\frac{f_c'}{f_0}\right)\left(\frac{c_0}{d_a}\right)^{1.7}\left(\frac{\rho_c}{\rho_0}\right)^{0.1}\right]^{-0.43}$;
$\phi = 21.6\left(\frac{f_t^*}{f_c^*}\right)^{-0.2}$	$\phi = 20.65\left(\frac{f_t^*}{f_c^*}\right)^{-0.21}$

(R^2) was obtained. Consequently, the simple equation for the v_c of LWAC-BS could be proposed as follows (Fig. 5):

$$v_c = 1.0EXP\left[-0.055\left(\frac{f_c'}{f_0}\right)\left(\frac{\rho_0}{\rho_c}\right)^{1.5}\right] \quad (1)$$

where f_0 (=10 MPa) and ρ_0 (=2300 kg/m^3) are the reference values for the compressive strength and dry density, respectively, of concrete.

The tensile strength of LWAC is marginally affected by the types of expanded lightweight aggregates and d_a (Choi et al. 2014) because the tensile fracture of LWAC is typically governed by the separation failure divided by a single crack penetrating aggregate particle. In addition, very few, if any, reliable model was studied in developing the tensile stress–strain relationship for LWAC, because the post-peak tensile behavior of concrete depends on the propagation of the tensile crack width. Yang et al. (2012) revised the tensile stress–strain relationship proposed by Hordijk's (1991) to account for a higher growth potential of crack opening in LWAC. Thus, the present study adopted the revised version (Yang et al. 2012) to determine the slopes of ascending and descending branches in tensile stress–strain relationship, at which the tensile strength was defined using the equation obtained empirically by Lee et al. (2019) for LWAC-BS. Overall, the effective strength ratio (f_t^*/f_c^*) of LWAC-BS required for the calculation of parameters l and m given in Table 4 could be solved in accordance with the numerical analysis approach by Kwon et al. using the aforementioned stress–strain relationships. From the parametric study conducted using the same variable ranges as that for deriving the simple equation of v_c, the value of f_t^*/f_c^* calculated for each concrete was formulated through the NLMR analysis of the numerical results. Overall, the f_t^*/f_c^* for LWAC-BS can be expressed in the following form (Fig. 6):

$$\frac{f_t^*}{f_c^*} = 0.11\left[\left(\frac{f_c'}{f_0}\right)^{0.8}\left(\frac{c_0}{d_a}\cdot\frac{\rho_0}{\rho_c}\right)\right]^{-0.83} \quad (2)$$

where c_0 (=25 mm) is the reference value for the maximum aggregate size.

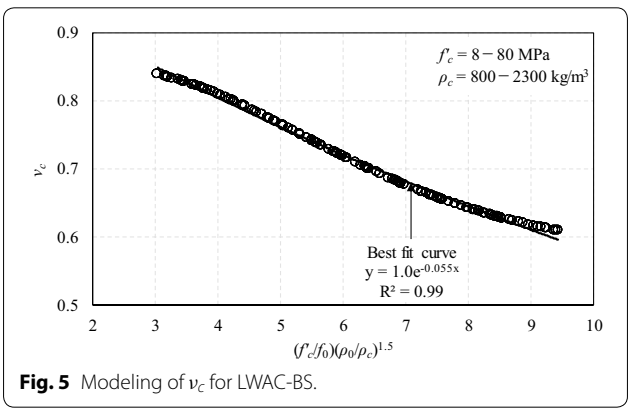

Fig. 5 Modeling of v_c for LWAC-BS.

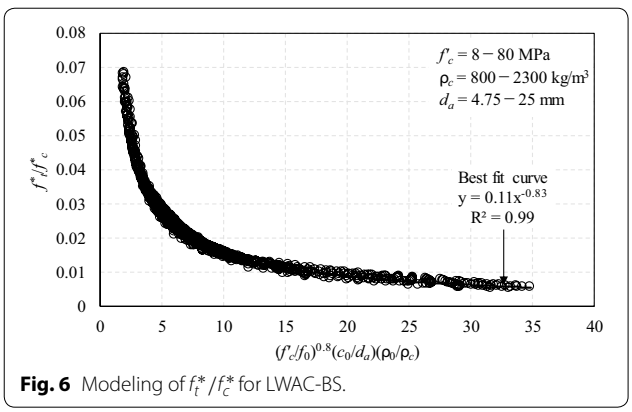

Fig. 6 Modeling of f_t^*/f_c^* for LWAC-BS.

Following the concrete plasticity (Nielsen and Hoang 2011) describing the energy dissipated in concrete along the sliding failure surface, frictional angle (ϕ) can be expressed as a function of f_t^*/f_c^* as follows:

$$\phi = \cos^{-1}\left(\frac{l - m\sin\alpha}{\cos\alpha}\sqrt{\frac{1+\sin\phi}{1-\sin\phi}}\right) \quad (3)$$

The variables of l and m in the equation above are defined as $1 - 2\frac{f_t^*}{f_c^*}\frac{\sin\phi}{1-\sin\phi}$ and $1 - 2\frac{f_t^*}{f_c^*}\frac{1}{1-\sin\phi}$, respectively. Hence, the solution of ϕ can be obtained from the numerical analysis for a given value of f_t^*/f_c^*. For the typical ranges of f_t^*/f_c^* (=0.005–0.07; see Fig. 6) of LWAC-BS, the ϕ values calculated from the numerical analysis can be formulated as follows (Fig. 7):

$$\phi = 21.6\left(\frac{f_t^*}{f_c^*}\right)^{-0.2} \quad (4)$$

Nielsen and Hoang (2011) regarded a constant ϕ value as 37°, regardless of $f_c^{'}$ and ρ_c, whereas Kahraman and Altindag (2004) demonstrated that the ϕ value depends on the material brittleness. Equation (4) also implies that the ϕ value increases with the increase in $f_c^{'}$ and decrease in ρ_c, followed by the decrease in the energy dissipation in the stress–strain curves.

LWAC-BS exhibits a slightly higher value of ϕ than LWAC-CF at the same $f_c^{'}$ and ρ_c, as shown in Fig. 8. The difference in ϕ values between two concrete types increases with the increase in $f_c^{'}$ and decrease in ρ_c. This is because LWAC-BS has a more rapid decreasing rate in the descending branch of the stress–strain curve in compression than LWAC-CF with the same $f_c^{'}$ and ρ_c (Lee et al. 2019). Meanwhile, the effect of d_a on the ϕ values is similar in two types of LWAC.

5.2 Verification of the Expanded Model

Figure 9 presents the comparisons of the measured τ_f of the present push-off specimens and those predicted using

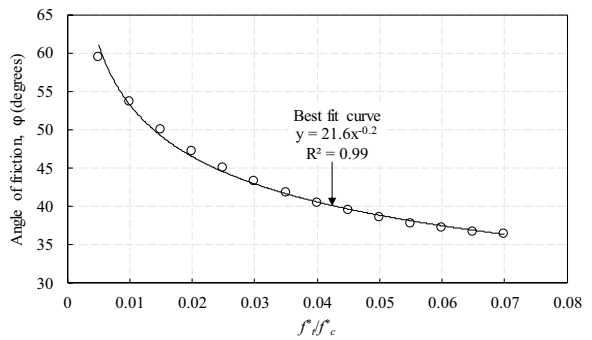

Fig. 7 Modeling of ϕ for LWAC-BS.

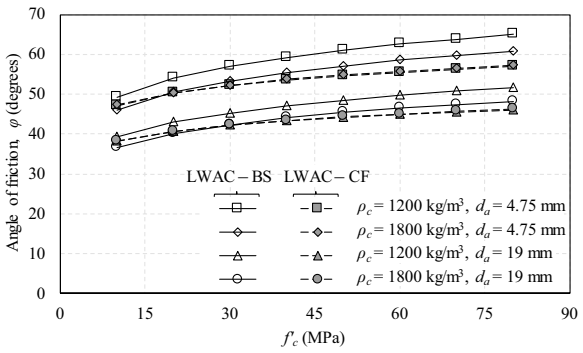

Fig. 8 Comparisons of ϕ values between LWAC-BS and LWAC-CF.

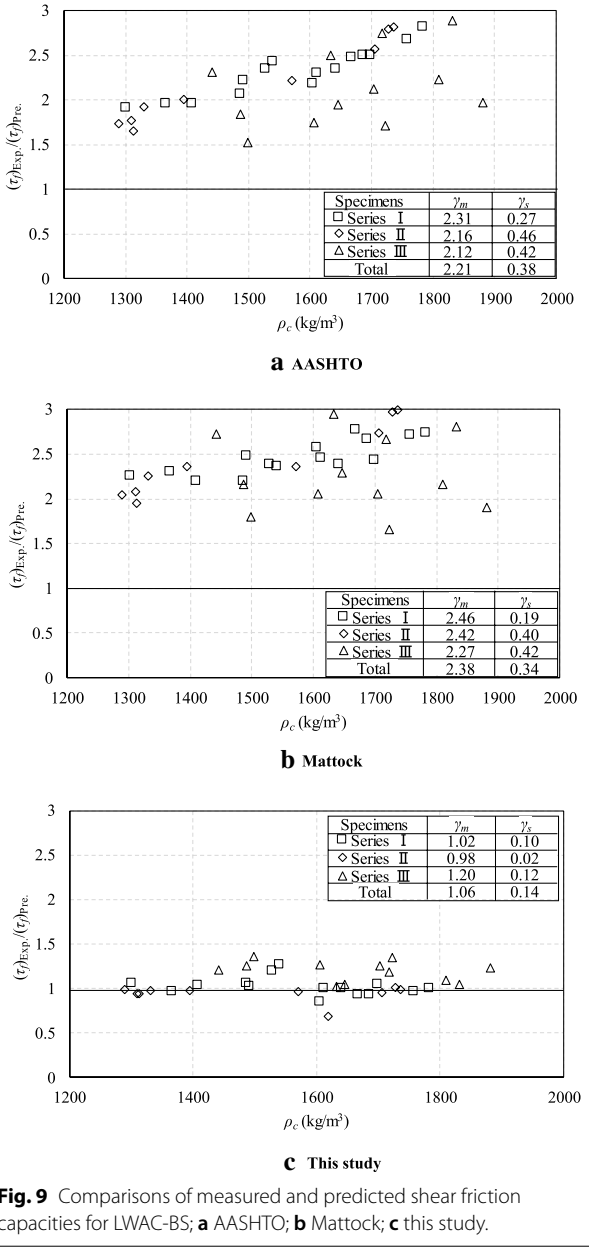

Fig. 9 Comparisons of measured and predicted shear friction capacities for LWAC-BS; **a** AASHTO; **b** Mattock; **c** this study.

the proposed mathematical model and the empirical equations of the AASHTO provision (2014) and Mattock (2001). In the same figure, the mean (γ_m) and standard deviation (γ_s) of the ratios (γ) between the measured and predicted values are also presented for comparisons. Additionally, these comparisons for each specimen are presented in Table 3. Note that γ values below 1.0 indicate an unsafe prediction of τ_f, whereas those exceeding 1.0 refer to an underestimation. The AASHTO equation highly underestimates the τ_f of LWAC-BS, resulting in a greater underestimation with the increase in ρ_c, $f_c^{'}$, and d_a. The values of γ_m and γ_s determined from the comparisons between the measured τ_f and the AASHTO equation are 2.21 and 0.38, respectively. This is because the AASHTO equation assigns the constant τ_f value of 1.65 MPa for LWAC interfaces without clamping forces that can be induced from transverse reinforcement and applied normal stresses. The equation by Mattock also gives quite underestimated results. According to Mattock's equation, the τ_f for a concrete interface without clamping forces is predicted as 1.7 MPa for sand-LWAC and 1.4 MPa for all-LWAC. The empirical equations of the AASHTO provision and Mattock were empirically fitted using extremely limited test data for the LWAC push-off specimens. Thus, they do not consider the influencing variables on the τ_f of the LWAC interfaces. The values of γ_m and γ_s determined from the comparisons were 2.38 and 0.34, respectively, for the Mattock equation. These values are very similar to those determined from the comparisons using the AASHTO equation.

The predictions from the model expanded in this study for LWAC-BS agree better with the test results, indicating the values of γ_m and γ_s of 1.06 and 0.14, respectively. The present models tend to underestimate the τ_f of LWAC interfaces; however, the degree of underestimation is significantly reduced when compared with the existing empirical equations. This implies that the shear friction parameters for LWAC-BS can be estimated using the equations derived from the expanded mechanism analysis, accounting for the reduced aggregate interlock capacity of such concrete. The present mechanical approach needs to further consider the effect of pre-cracks or crack inducers along the shear plane on the frictional angle of LWAC because shrinkage cracks are likely to be developed in practical concrete interfaces.

6 Modification Factor

According to the ACI 318-14 provision (2014), the modification factor (λ) is defined as a ratio of shear transfer capacity of LWAC to that of the companion NWC. As the λ is introduced to account for the reduced frictional properties along the crack interfaces in LWAC, the following equation can be identified:

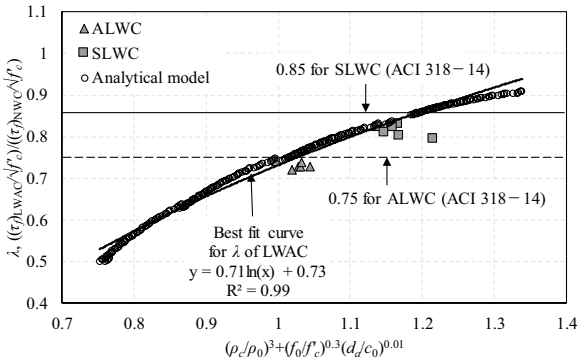

Fig. 10 Generalization of modification factor for LWAC-BS.

$$\lambda = \frac{(\tau_f)_{LWAC}}{(\tau_f)_{NWC}} \tag{5}$$

To calculate the value of λ using the equations for τ_f summarized in Table 4 and Eq. (5), a numerical parametric study was conducted for different concrete specimens with $f_c^{'}$ ranging from 8 and 80 MPa, d_a ranging from 4.75 mm and 25 mm, and ρ_c between 800 and 2300 kg/m^3. The concrete specimens with ρ_c of 2300 kg/m^3 indicate NWC. The results obtained from the parametric study were formulated by the regression analysis approach, as plotted in Fig. 10; therefore, a modification factor for LWAC-BS can be finally proposed:

$$\lambda = 0.71 \ln\left[\left(\frac{\rho_c}{\rho_0}\right)^3 + \left(\frac{f_0}{f_c^{'}}\right)^{0.3}\left(\frac{d_a}{c_0}\right)^{0.01}\right] + 0.73 \tag{6}$$

Figure 10 shows the comparisons of the measured λ values and predictions by the equation above. To examine the reliability of Eq. (6), NWC push-off specimens were additionally tested at the same parameters as the series III specimens. When determining the λ values, τ_f is normalized by the square root of $f_c^{'}$ to neglect the inevitable difference of $f_c^{'}$ between the NWC and LWAC push-off specimens at the same test parameters. The predicted λ values are in relatively good agreement with the test results. Unlike the constant λ values specified in the ACI 318-14 provision, the λ values calculated from the proposed equation tend to decreases with the increase in $f_c^{'}$ and the decrease in ρ_c. The ACI 318-14 provision tends to overestimate the λ values for LWAC-BS. Additionally, the predicted λ values are slightly influenced by d_a. Thus, it can be concluded that the proposed modification factor rationally explains

the reduced frictional properties along the shear crack interfaces.

7 Conclusions

From the extensive tests and expanded mathematical models to assess the shear friction characteristic at the monolithic concrete interfaces made using artificially expanded bottom ash and dredged soil granules, the following conclusions may be drawn:

1. The normalized shear friction strength ($\tau_f/f_c^{'}$) of LWAC increased with the increase in sand contend (R_s) for the replacement of lightweight fine aggregates; however, the increasing rate of $\tau_f/f_c^{'}$ with respect to R_s was independent of the compressive strength of concrete ($f_c^{'}$).
2. The value of $\tau_f/f_c^{'}$ tended to decrease with the increase in $f_c^{'}$ at the same level of dry density (ρ_c) of concrete.
3. The increasing rate in $\tau_f/f_c^{'}$ with respect to the maximum size of aggregate (d_a) was similar in both sand-LWAC and all-LWAC specimens. When d_a varied from 4.75 mm to 19 mm, the increasing rates of $\tau_f/f_c^{'}$ were 131–137% for the all-LWAC and 137–140% for the sand-LWAC.
4. The frictional angle (ϕ) of concrete using expanded bottom ash and dredged soil granules was estimated to be slightly higher than that of concrete using expanded clay and fly ash granules.
5. The empirical equations proposed by the AASHTO provision and Mattock underestimated significantly the τ_f of concrete using expanded bottom ash and dredged soil granules, resulting in a greater underestimation with the increase in ρ_c, $f_c^{'}$, and d_a. Meanwhile, the predictions obtained from the present mathematical model agreed better with the test results, in which the mean and standard deviation of the ratios between the measured and estimated shear friction strengths were 1.06 and 0.14, respectively.
6. The modification factor determined from the mathematical models for the shear friction strength of the concrete interface agreed relatively well with the test results, unlike the overestimation trend observed in the ACI 318-14 provision.

Abbreviations

All-LWAC: concrete in which both the coarse- and fine-aggregate components are lightweight aggregates; LWAC: lightweight aggregate concrete; LWAC-BS: lightweight aggregate concrete made using expanded bottom ash and dredged soil granules; LWAC-CF: lightweight aggregate concrete made using expanded clay and/or fly ash granules; NLMR: non-linear multiple regression; NWC: normal-weight concrete; OPC: Ordinary Portland cement; Sand-LWAC: concrete with coarse lightweight aggregate and fine normal-weight aggregate.

Acknowledgements

This work was supported by the National Research Foundation of Korea (NRF) grant funded by the Korea Government (MSIP) (No. NRF-2017R1A2B3008463) and Basic Science Research Program through NRF Funded by the Ministry of Science, ICT & Future Planning (No. 2015R1A5A1037548).

Authors' contributions

All the authors contributed to this research with respect to the followings: the first and second authors designed the present experimental program and conducted testing; and the second author also derived the mathematical model. All authors read and approved the final manuscript.

Funding

Not applicable.

Availability of data and materials

Not applicable.

Ethics approval and consent to participate

Not applicable.

Consent for publication

Not applicable.

Competing interests

The authors declare that they have no competing interests.

Received: 8 December 2018 Accepted: 2 August 2019
Published online: 14 October 2019

References

AASHTO. (2014). *AASHTO LRFD Bridge design specifications* (7th ed.). Washington, DC: American Association of State Highway and Transportation Official.

ACI Committee 213. (2014). *Guide for structural lightweight-aggregate concrete (ACI 213R-14)*. American Concrete Institute.

ACI Committee 318. (2014). *Building code requirements for structural concrete and commentary (ACI 318-14)*. Farmington Hills, MI: American Concrete Institute.

ACI-ASCE Committee 426. (1973). The shear strength of reinforced concrete members. *Journal Proceedings, 70*(7), 471–473.

ASTM C39, C143, C150, C231, C330, C642. (2013). *Annual book of ASTM standards: V. 4.02*. ASTM International.

Choi, S. J., Yang, K. H., Sim, J. I., & Choi, B. J. (2014). Direct tensile strength of lightweight concrete with different specimen depths and aggregate sizes. *Construction and Building Materials, 63,* 132–141.

EN 1992-1-1 (2004). *Eurocode 2—design of concrete structures—Part 1: General rules and rules for buildings*. Brussels, Belgium: European Committee for Standardization.

fib (2010). *Model code for concrete structures 2010: Special activity group 5*. Switzerland, Lausanne: Fédération Internationale de B´eton.

Hordijk, D. A. (1991). *Local Approach to Fatigue of Concrete. Doctoral dissertation*. Delft: Netherlands. Delft University of Technology.

Ivey, D. I., & Buth, E. (1967). Shear capacity of lightweight concrete beams. *ACI Journal Proceedings, 161*(10), 634–643.

Kahraman, S., & Altindag, R. (2004). A brittleness index to estimate fracture toughness. *International Journal of Rock Mechanics and Mining Sciences, 41*(1), 343–348.

Kwon, S. J., Yang, K. H., Hwang, Y. H., & Ashour, A. F. (2017). Shear friction strength of monolithic concrete interfaces. *Magazine of Concrete Research, 69*(5), 230–244.

Lee, J. H., & Hong, S. G. (2015). Shear friction strength on limit analysis for ultra-high performance fiber reinforced concrete. *Journal of the Korea Concrete Institute, 27*(3), 299–309.

Lee, K. H., Yang, K. H., Mun, J. H., & Kwon, S. J. (2019). Mechanical properties of concrete made from different expanded lightweight aggregates. *ACI Structural Journal, 116*(2), 9–19.
Mattock, A. H. (2001). Shear friction and high-strength concrete. *ACI Structural Journal, 98*(1), 50–59.
Mattock, A. H., Li, W. K., & Wang, T. C. (1976). Shear transfer in lightweight reinforced concrete. *PCI Journal, 21*(1), 20–39.
Nielsen, M. P., & Hoang, L. C. (2011). *Limit analysis and concrete plasticity*. England: Prentice-Hall.
Shaikh, A. F. (1978). Proposed revisions to shear-friction provisions. *PCI Journal, 23*(2), 12–21.
Tang, W. C., Lo, T. Y., & Chan, W. K. (2008). Fracture properties of normal and lightweight high-strength concrete. *Magazine of Concrete Research, 60*(4), 237–244.
Yang, K. H., & Ashour, A. F. (2011). Aggregate interlock in lightweight concrete continuous deep beams. *Engineering Structures, 33*(1), 136–145.
Yang, K. H., & Ashour, A. F. (2015). Modification factor for lightweight concrete beams. *ACI Structural Journal, 112*(4), 485–492.
Yang, K. H., Kim, G. H., & Choi, Y. H. (2014a). An initial trial mixture proportioning procedure for structural lightweight aggregate concrete. *Construction and Building Materials, 55,* 431–439.
Yang, K. H., Mun, J. H., Cho, M. S., & Kang, T. H. K. (2014b). A stress–strain model for various unconfined concrete in compression. *ACI Structural Journal, 111*(4), 819–826.
Yang, K. H., Sim, J. I., Kang, J. H., & Ashour, A. F. (2012). Shear capacity of monolithic concrete joints without transverse reinforcement. *Magazine of Concrete Research, 64*(9), 767–779.

Publisher's Note